Supporting Information

Park et al. 10.1073/pnas.1300021110

SI Materials and Methods

Mice. All procedures were approved by the Institutional Animal Care and Use Committee of Weill Cornell Medical College. All experiments were performed in male mice of three age groups: 3, 18, and 22 mo. The method for crossing amyloid precursor protein (APP) mice with $CD36^{0/0}$ mice was identical to that described by Park et al. (1). In brief, transgenic mice overexpressing the Swedish mutation of the APP Tg2576 (APP_{Swe}) (2) were bred with $CD36^{0/0}$ mice (3). The targeted null allele is on a C57BL/6J background (N9), whereas the APP_{Swe} transgene array is congenic on a 129S6 background (N21). Therefore, to minimize confounding effects attributable to background heterogeneity and genetic modifiers, experiments were performed in age-matched littermates. For this, 129.Tg(APP_{Swe})2576 mice hemizygous for the transgene array (APP_{Swe}^{+}/APP_{Swe}^{-}) were crossed with B6.129-$CD36^{tm1Mfe}$ mice homozygous for the CD36 null allele (designated $^{0/0}$) to produce $CD36^{0/wt}$ mice carrying the APP transgene. (The transgene insertion site and CD36 are on different chromosomes.) APP_{Swe}^{+} $CD36^{0/wt}$ F1 mice were backcrossed to $CD36^{0/0}$ mice to produce APP_{Swe}^{+} $CD36^{0/0}$, APP_{Swe}^{+} $CD36^{0/wt}$, APP_{Swe}^{-} $CD36^{0/0}$, and APP_{Swe}^{-} $CD36^{0/wt}$ mice. PCR was used to genotype the APP transgene array as described previously (1, 4). No $CD36^{wt/wt}$ mice were produced from this cross. To produce APP_{Swe}^{+} mice and controls that were $CD36^{wt/wt}$ for comparison with $CD36^{0/0}$ and $CD36^{0/+}$ littermates, APP^{+} $CD36^{0/wt}$ and APP^{-} $CD36^{0/wt}$ F1 mice were intercrossed. CBF results did not differ between the offspring of C57BL/6J-Tg2576 and 129S6. Tg2576 males.

General Surgical Procedures. Mice were anesthetized with isoflurane [maintenance 2% (vol/vol)], intubated, and artificially ventilated (SAR-830; CWE) (1, 4). The femoral vessels were cannulated for recording of arterial pressure and blood gas analysis. Rectal temperature was maintained at 37 °C. After surgery, anesthesia was maintained with urethane (750 mg/kg i.p.) and chloralose (50 mg/kg i.p.) (1, 4–6).

Cerebral Blood Flow and Cerebrovascular Reactivity. A craniotomy (2 × 2 mm) was performed to expose the somatosensory cortex, the dura was removed, and the site was superfused with modified Ringer's solution (pH 7.3–7.4) at 37 °C (1, 4–6). Cerebral blood flow (CBF) was monitored at the site of superfusion with a laser Doppler probe (Vasamedic) positioned stereotaxically on the brain surface and connected to a computer. CBF was expressed as percentage increase relative to the resting level (1, 4–6).

Experimental Protocol for CBF Experiments. CBF recordings were started after arterial pressure and blood gas values were at steady state (Table S1). All pharmacologic agents studied were dissolved in Ringer's solution unless noted otherwise. To study the increase in CBF produced by somatosensory activation, the whiskers were activated by side-to-side deflection for 60 s The endothelium-dependent vasodilators acetylcholine (10 μM), bradykinin (50 μM), and A23187 (3 μM) (all Sigma-Aldrich) were topically superfused for 3–5 min, and the resulting changes in CBF were monitored (5, 6). The response of CBF to the smooth muscle relaxants SNAP (50 μM) and adenosine (400 μM) (both from Sigma-Aldrich) and to hypercapnia (pCO_2 50–60 mmHg) was examined as well (1, 4).

Measurement of Aβ. Aβ was measured using an ELISA-based assay, as described previously (1, 4, 7). In brief, left hemispheres of the mice used for CBF studies were sonicated in 1% (wt/vol) SDS with protease inhibitors and centrifuged. The supernatant contained SDS-soluble Aβ peptides. The pellet was sonicated in 70% (vol/vol) formic acid (FA) and centrifuged as above. The FA extract was neutralized by a 1:20 dilution into 1 M Tris phosphate buffer (pH 8.0). Aβ1-40 and Aβ1-42 concentrations (picomoles per gram of brain tissue) were determined in supernatant (SDS-soluble) and the FA acid extract of the pellet (SDS-insoluble), using BAN-50/BA-27 and BAN-50/BC005 sandwich ELISA as described previously (1, 4, 7).

General Procedures for Immunofluorescence and Confocal Imaging. Mice were anesthetized with sodium pentobarbital (150 mg/kg i.p.) and perfused transcardially with heparinized saline, followed by 4% (wt/vol) paraformaldehyde (PFA) (1, 4, 8). Brains were removed, postfixed, and sectioned (40 μm) with a vibratome. Free-floating sections were selected at random and processed for labeling. The specificity of immunolabeling was established by omitting the primary antibody or performing preabsorption with the antigen. Random images were acquired with a Leica SP5 laser scanning confocal microscope in the somatosensory cortex underlying the cranial window (0.38 to −1.94 mm from the bregma) (9). Brain sections from Tg2576/$CD36^{wt/wt}$ and Tg2576/$CD36^{0/0}$ (n = 5/group) were processed under identical conditions and imaged using identical settings. As detailed below, each parameter was quantified using ImageJ.

Determination of Aβ Load. Aβ load was determined by immunohistochemistry and stereological image analysis as described previously (4). In brief, right hemispheres of Tg-2576/$CD36^{wt/wt}$ and Tg2576/$CD36^{0/0}$ mice used for the CBF studies (n = 5 per group) were postfixed in 4% PFA. Coronal sections were andomly selected for immunocytochemistry, using an Aβ antibody (1:1,000, 4G8; Sigma-Aldrich). Gray-scale images (1× magnification) of the cortex and hippocampus were digitized with a camera (QImaging; Barnaby). Using ImageJ, the number of plaques per square millimeter was counted in the cortex and hippocampus, and the Aβ load was determined from the area occupied by the plaques relative to the total area of cortex or hippocampus, in a blinded manner.

Cerebral Amyloid Angiopathy Burden and Smooth Muscle Cell Fragmentation. *Cerebral amyloid angiopathy burden.* Brain sections were first incubated with α-actin (1:300, rabbit polyclonal; Abcam) or Aβ1-40 (1:100, mouse; Covance) antibody for 48 h, followed by cyanine dye (Cy)5-conjugated anti-rabbit or anti-mouse secondary IgG (1:200, Jackson ImmunoResearch). After mounting on slides and refixation with 4% PFA for 10 min, brain sections were washed and labeled with 0.05% (wt/vol) thioflavine-S in 50% (vol/vol) ethanol for 10 min to identify cerebral amyloid angiopathy (CAA). Confocal images were obtained with an FITC filter for thioflavine-S and a Cy5 filter for α-actin or Aβ1-40. Merged images of thioflavine-S and α-actin were acquired and quantified, and the CAA burden was expressed by the ratio (%) of the number of neocortical vessels positive for both thioflavine-S and α-actin divided by the total number of $\alpha\text{-actin}^{+}$ vessels (10, 11). Some sections were coincubated with anti-Aβ (4G8; Sigma-Aldrich) and the basement membrane marker anti-collagen IV (Col IV; 1:500, rabbit; Abcam) for 24 h, followed by donkey FITC-conjugated anti-mouse or Cy5-conjugated anti-rabbit IgG (1:200; Jackson ImmunoResearch). Images were acquired by confocal microscopy.

Fragmentation of smooth muscle cells. To quantify Aβ-associated fragmentation of smooth muscle cells, brain sections were incubated with anti-Aβ (4G8, 1:1,000, mouse; Covance) and the smooth muscle marker anti–α-actin (1:300, rabbit; Abcam) for 48 h. After washing, sections were labeled with donkey FITC-conjugated anti-mouse or Cy5-conjugated anti-rabbit IgG (1:200; Jackson ImmunoResearch). Neocortical arterioles (n = 40–60/group) positive for both Aβ and α-actin, ranging in diamter from 20 to 100 μm, were randomly imaged by confocal microscopy (60×). The fragmentation of smooth muscles was quantified by counting the number of α-actin fragments of each arteriole using ImageJ, expressed as the fragmentation index: 100 − [(1/number of α-actin fragments) × 100].

Pericyte Assessment by Immunofluorescence and EM. ***Immunofluorescence.*** Brain sections were processed for immunofluorescence staining with anti-Col IV (1:500, rabbit; Abcam) and pericyte marker anti–platelet-derived growth factor receptor-β (PDGFR-β; 10 μg/mL, goat; R&D Systems) antibodies overnight. These sections were then incubated with donkey FITC-conjugated anti-rabbit or Cy5-conjugated anti-goat IgG. Once merged confocal images were acquired, PDGFR-β^+ cell bodies were counted using ImageJ and expressed as number of PDGFR-β^+ cell bodies per square millimeter.

EM. Anesthetized mice were perfused transcardially with 2% (vol/vol) heparin saline, 3.75% (wt/vol) acrolein, and 2% PFA in phosphate buffer. Brains were postfixed for 30 min in 2% PFA in phosphate buffer, and random 40-μm-thick sections through the primary somatosensory cortex were dehydrated, postfixed in 2% osmium for 1 h, and then embedded in Embed 812 (Electron Microscopy Sciences) (8). Random portions of the primary somatosensory cortex were excised, and thin sections (65 nm) were collected and counterstained before examination on a Tecnai electron microscope (FEI) (8). Digital images of all capillary profiles (with diameter <10 μm) in randomly selected thin sections were acquired; 143 vessels were quantified for WT mice, and 130 vessels were quantified for Tg-2576/CD36$^{wt/wt}$ mice (n = 3/group). The resulting micrographs were analyzed in terms of percent pericyte coverage, defined as the portion of the perimeter of the capillary profile occupied by pericytic processes divided by total capillary profile perimeter. Pericytic processes were identified by complete embedment within the basement membrane (12).

LRP-1 and ZO-1 Immunofluorescence. Brain sections were processed for immunofluorescence staining with anti-Col IV (1:500; Abcam) and anti–low-density lipoprotein receptor-related protein-1 (LRP-1; 5 μg/mL, mouse; LifeSpan Biosciences) overnight. Sections were incubated with donkey FITC-conjugated anti-rabbit or Cy5-conjugated anti-mouse IgG. Confocal images were acquired and quantified for the area occupied by Col IV$^+$ or LRP-1$^+$ blood vessels separately using ImageJ, and LRP-1 was assessed as a ratio (%) of LRP-1$^+$ area divided by Col IV$^+$ area of blood vessels. For ZO-1 immunofluorescence, brain sections were incubated with endothelial cell marker CD31 antibodies (1:50, rat; BD Biosciences) and tight junction protein ZO-1 antibodies (3 μg/mL, mouse; Invitrogen) overnight. Sections were then incubated with donkey FITC-conjugated anti-rat or Cy5-conjugated anti-mouse IgG. Confocal images were obtained and quantified for areas occupied by ZO-1$^+$ or CD31$^+$ blood vessels separately using ImageJ, and ZO-1 quantification was expressed as a ratio (%) of ZO-1$^+$ area divided by CD31$^+$ cortical vessels.

Assessment of Microglia. Random brain sections were incubated with microglial marker rabbit Iba-1 antibodies (1:500; Wako) for 48 h. After washing, the sections were incubated with Cy5-conjugated donkey anti-rabbit IgG (1:200; Jackson ImmunoResearch). Confocal images of random fields of Iba-1$^+$ microglia within the somatosensory cortex were obtained, and the number of Iba-1$^+$ microglial cells was counted using ImageJ and expressed as the number of Iba-1$^+$ microglia per square millimeter. For determination of CAA-associated microglia, random brain sections were double-labeled for thioflavine-S and the microglial marker Iba-1. Sections were first incubated with anti- Iba-1 (1:500; Wako) for 48 h, followed by Cy5-conjugated anti-rabbit IgG (1:200; Jackson ImmunoResearch). After mounting on slides and refixation with 4% PFA for 10 min, sections were washed and labeled with 0.05% thioflavine-S in 50% ethanol for 10 min. Under confocal microscopy, thioflavine-S$^+$ CAAs (n = 30–40/group) were identified, and merged images of CAA and Iba-1$^+$ microglia were obtained using the appropriate filters. The number of CAA-associated Iba-1$^+$ microglia was analyzed and expressed as a function of distance from the center of the CAA (Fig. S4) (13). For determination of plaque-associated microglia, random brain sections were double-labeled for anti–Iba-1 and anti-Aβ (4G8) for 48 h, followed by FITC-conjugated anti-mouse or Cy5-conjugated anti-rabbit IgG (1:200; Jackson ImmunoResearch). Under confocal microscopy, Aβ plaques were identified and categorized by size into two groups: 150–500 μm diameter and 501–1,000 μm diameter. Images positive for both Aβ plaques and Iba-1$^+$ microglia (n = 40–50/group) were acquired and quantified. The number of Aβ plaque-associated Iba-1$^+$ microglia was determined using ImageJ and expressed as a function of distance from the center of Aβ plaques (Fig. S5) (13).

Behavioral Assessment Using the Y Maze. Behavioral assessment was performed using the Y maze, as described previously (4). In brief, the Y maze consisted of three identical arms made of transparent plastic joined in the middle to form a "Y" (20 cm high, 10 cm wide, and 30 cm long). The mice were handled daily and allowed to acclimate to the apparatus for 1 wk before testing.

For the training trial, a mouse was placed into one arm of the maze (start arm) and allowed to explore only two of the arms for 5 min. The third arm, which remained closed, was chosen at random in each trial. For the test trial, the closed arm was opened, serving as the novel arm. After a 30-min intertrial interval, the mouse were returned to the same start arm and was allowed to explore all three arms for 5 min. Sessions were videorecorded and replayed for determination of the parameters of interest by an observer blinded to mouse genotype.

Data Analysis. Data are expressed as mean ± SEM. Two-group comparisons were analyzed using the two-tailed t test. Multiple comparisons were evaluated by ANOVA and the Tukey test. Differences in novel arm entries were analyzed using the χ^2 test. Differences were considered statistically significant at $P < 0.05$.

1. Park L, et al. (2011) Scavenger receptor CD36 is essential for the cerebrovascular oxidative stress and neurovascular dysfunction induced by amyloid-beta. *Proc Natl Acad Sci USA* 108(12):5063–5068.
2. Hsiao K, et al. (1996) Correlative memory deficits, Abeta elevation, and amyloid plaques in transgenic mice. *Science* 274(5284):99–102.
3. Febbraio M, et al. (1999) A null mutation in murine CD36 reveals an important role in fatty acid and lipoprotein metabolism. *J Biol Chem* 274(27):19055–19062.
4. Park L, et al. (2008) Nox2-derived radicals contribute to neurovascular and behavioral dysfunction in mice overexpressing the amyloid precursor protein. *Proc Natl Acad Sci USA* 105(4):1347–1352.
5. Iadecola C, et al. (1999) SOD1 rescues cerebral endothelial dysfunction in mice overexpressing amyloid precursor protein. *Nat Neurosci* 2(2):157–161.
6. Niwa K, et al. (2000) Abeta 1-40-related reduction in functional hyperemia in mouse neocortex during somatosensory activation. *Proc Natl Acad Sci USA* 97(17):9735–9740.
7. Kawarabayashi T, et al. (2001) Age-dependent changes in brain, CSF, and plasma amyloid (beta) protein in the Tg2576 transgenic mouse model of Alzheimer's disease. *J Neurosci* 21(2):372–381.
8. Pierce JP, et al. (2009) Sex differences in the subcellular distribution of angiotensin type 1 receptors and NADPH oxidase subunits in the dendrites of C1 neurons in the rat rostral ventrolateral medulla. *Neuroscience* 163(1):329–338.

9. Franklin K, Paxinos G (1997) *The Mouse Brain in Stereotaxic Coordinates* (Academic, San Diego).
10. Van Dooren T, et al. (2006) Neuronal or glial expression of human apolipoprotein e4 affects parenchymal and vascular amyloid pathology differentially in different brain regions of double- and triple-transgenic mice. *Am J Pathol* 168(1): 245–260.
11. Winkler DT, et al. (2001) Spontaneous hemorrhagic stroke in a mouse model of cerebral amyloid angiopathy. *J Neurosci* 21(5):1619–1627.
12. Díaz-Flores L, et al. (2009) Pericytes: Morphofunction, interactions and pathology in a quiescent and activated mesenchymal cell niche. *Histol Histopathol* 24(7):909–969.
13. Frautschy SA, et al. (1998) Microglial response to amyloid plaques in APPsw transgenic mice. *Am J Pathol* 152(1):307–317.

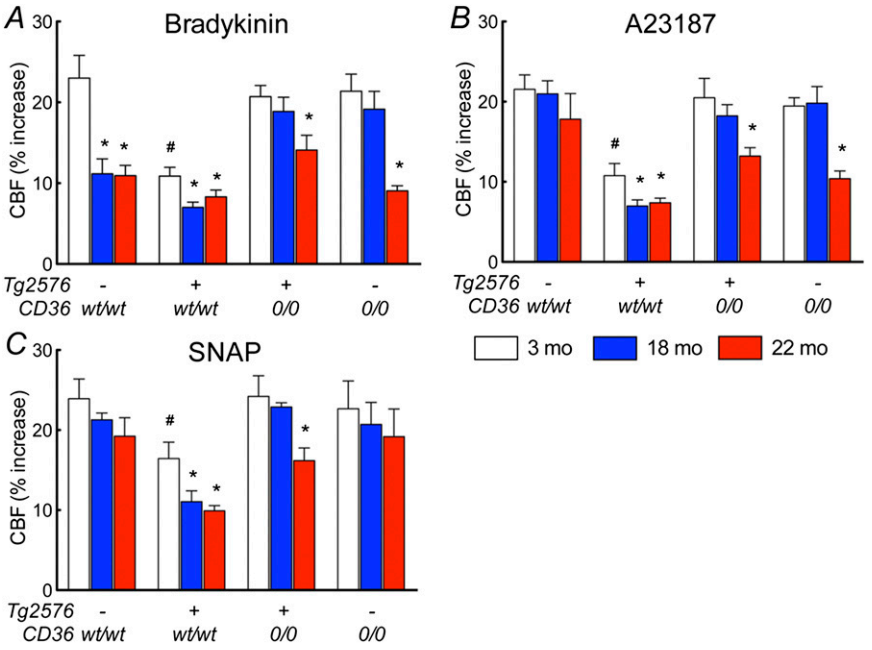

Fig. S1. CD36 deletion improves neurovascular function in Tg2576 mice at age 3 mo, 18 mo, and 22 mo ($n = 5$/group). CD36 deletion improves attenuation in the increase in CBF produced by the endothelium-dependent vasodilators bradykinin (*A*) and A23187 (*B*) and by the nitric oxide donor smooth muscle relaxant SNAP (*C*). The attenuation in CBF increase induced by aging in $CD36^{wt/wt}$ littermates is also ameliorated by CD36 deletion. $^{*}P < 0.05$ from 3 mo; $^{\#}P < 0.05$ from $CD36^{wt/wt}$, ANOVA and Tukey test.

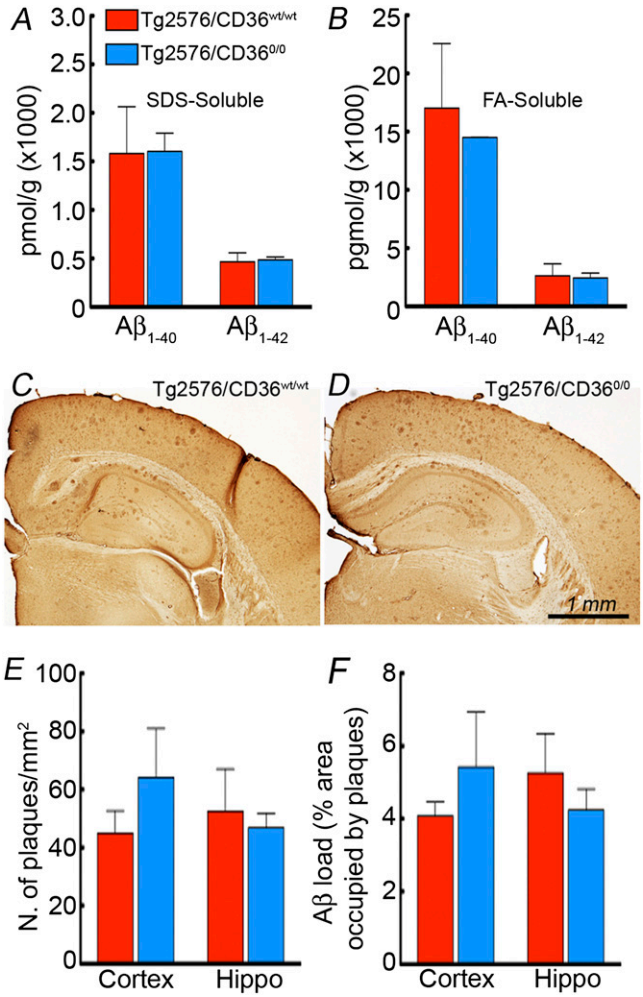

Fig. S2. CD36 deletion does not attenuate Aβ1-40, Aβ1-42, or plaque load in 22-mo-old Tg2576 mice. (*A* and *B*) SDS-soluble (*A*) and FA-soluble (SDS-insoluble) (*B*) Aβ1-40 and Aβ1-42 are not reduced in Tg2576/CD36$^{0/0}$ mice (n = 5/group; $P > 0.05$). (*C*–*F*) The distribution of amyloid plaques, assessed using 4G8 immunocytochemistry (*C* and *D*), and the number per square nillimeter (*E*) and percent occupied area (*F*) do not differ between Tg2576/CD36$^{wt/wt}$ and Tg2576/CD36$^{0/0}$ mice (n = 4–5/group; $P > 0.05$).

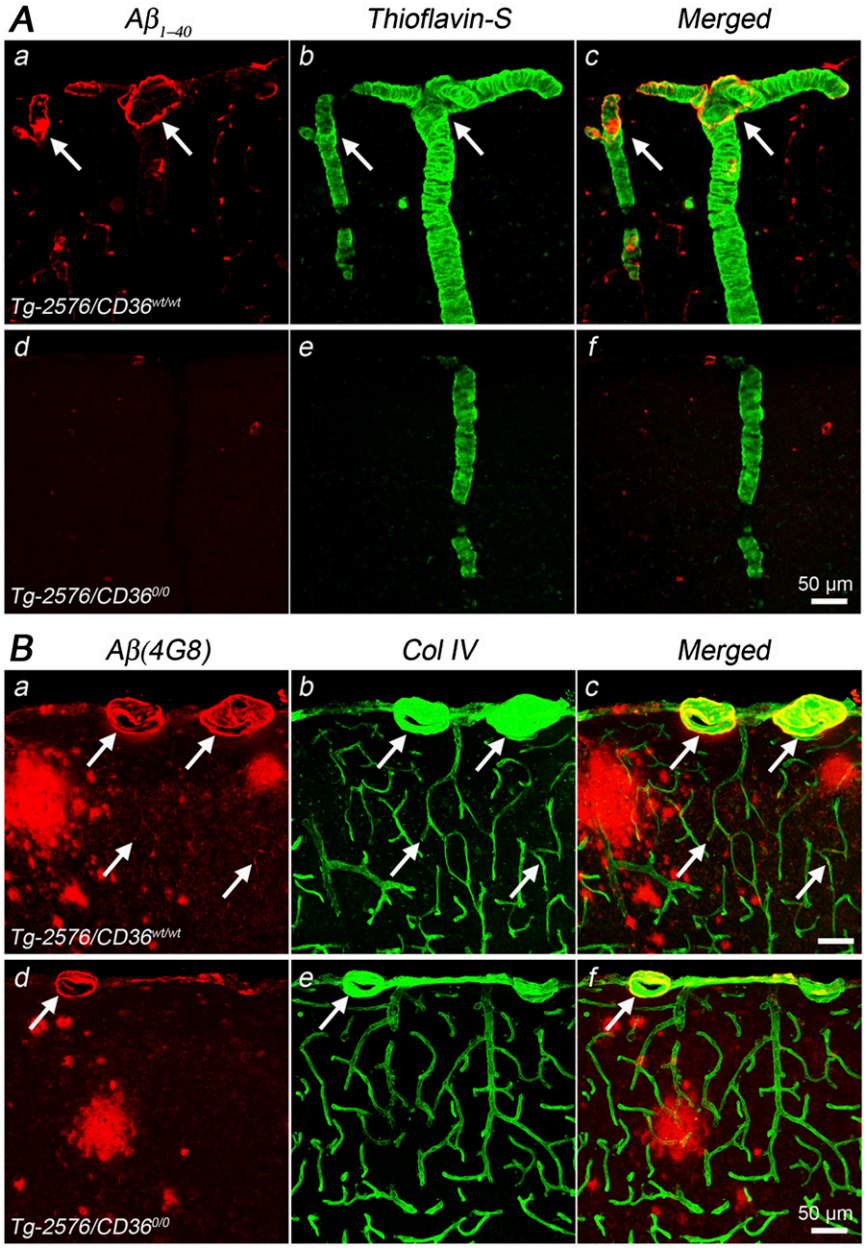

Fig. S3. CD36 deletion selectively attenuates CAA in cerebral arterioles in 18 mo-old Tg2576 mice. (*A*) In Tg2576/CD36$^{wt/wt}$ mice, pial and penetrating arterioles are positive for thioflavin-S and Aβ1-40 immunoreactivity (*a–c*). Both thioflavin-S and Aβ1-40 immunoreactivity are reduced in Tg2576/CD36$^{0/0}$ mice (*d–f*). (*B*) Association between Aβ and cerebral microvessels, identified by Col IV immunostaining, is observed in Tg2576/CD36$^{wt/wt}$ mice (*a–c*) but reduced in Tg2576/CD36$^{0/0}$ mice (*d–f*).

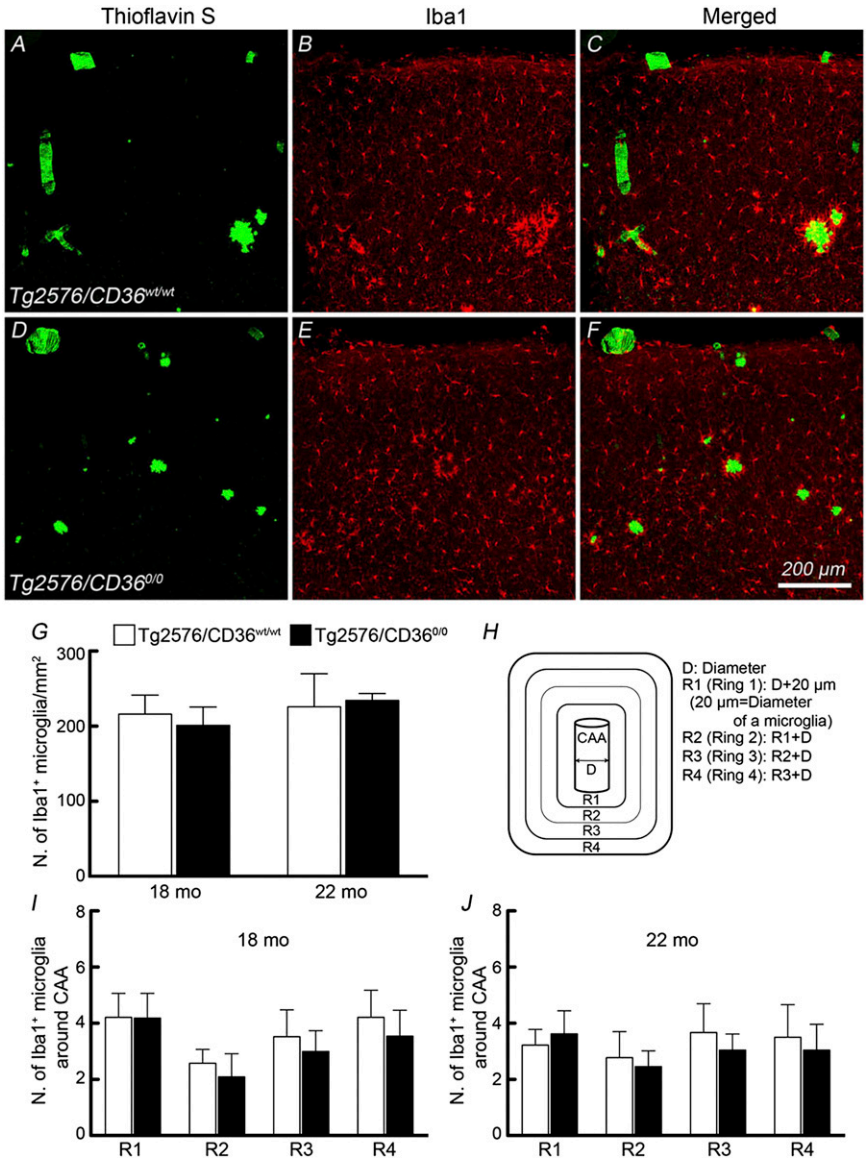

Fig. S4. CD36 deletion in Tg2576 mice does not alter the association between microglia and CAA. The association between thioflavin-S$^+$ vascular profiles and Iba-1$^+$ cells (microglia) is similar in Tg2576/CD36$^{wt/wt}$ mice (*A–C*) and Tg2576/CD36$^{0/0}$ mice (*D–F*), and the number of Iba-1$^+$ cells does not differ in these two groups (*G*) (n = 4–5/group; $P > 0.05$). (*H–J*) The number of Iba-1$^+$ cells was quantified at increasing distances from thioflavin-S$^+$ vessels, corresponding to one, two, three, or four vessel diameters. The first ring (R1) was arbitrarily set to correspond to the vessel diameter plus the average diameter of an Iba-1$^+$ cell (*H*). The number of Iba-1$^+$ cells at the different distances from the vessels (R1, R2, R3, and R4) is similar in Tg2576/CD36$^{wt/wt}$ and Tg2576/CD36$^{0/0}$ mice at 18 mo (*I*) and 22 mo (*J*) (n = 4–5/group; $P > 0.05$).

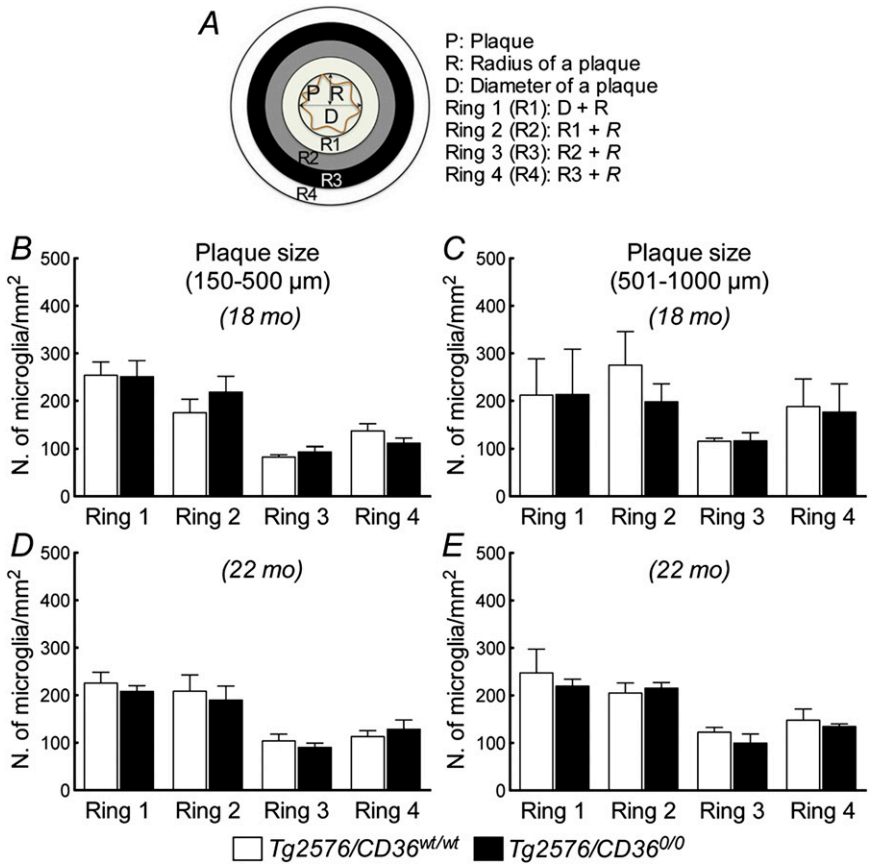

Fig. S5. CD36 deletion in Tg2576 mice does not alter the association between microglia and amyloid plaques. (*A*) The number of Iba-1$^+$ cells was quantified at increasing distances (R1–R4) from amyloid plaques identified by 4G8 immunocytochemistry. The first ring was set arbitrarily to a distance corresponding to the diameter plus the radius of a plaque. The other rings corresponded to the distance of the previous ring plus the plaque diameter. (*B–E*) No difference in the number of Iba-1$^+$ cells associated with the plaques was observed between Tg2576/CD36$^{wt/wt}$ and Tg2576/CD36$^{0/0}$ mice for two different plaque sizes at age 18 mo (*B* and *C*) or age 22 mo (*D* and *E*) (n = 4–5/group; $P > 0.05$).

Table S1. Arterial pressure and blood gas values in the mice with CBF measurements

Vasoactive stimuli/age	Genotype	MAP, mmHg	pCO_2, mmHg	pO_2, mmHg	pH	*n*
Whisker stimulation, ACh, adenosine						
3 mo	$CD36^{wt/wt}$	82 ± 2	31.3 ± 1.3	136.8 ± 4.6	7.39 ± 0.01	5
	$Tg2576/CD36^{wt/wt}$	82 ± 3	31.8 ± 1.6	135.8 ± 6.3	7.38 ± 0.02	5
	$Tg2576/CD36^{0/0}$	81 ± 4	33.7 ± 2.3	132.9 ± 8.7	7.37 ± 0.02	5
	$CD36^{0/0}$	82 ± 2	33.3 ± 2.4	133.7 ± 8.5	7.36 ± 0.02	6
18 mo	$CD36^{wt/wt}$	81 ± 2	36.1 ± 1.3	130.4 ± 5.0	7.39 ± 0.02	5
	$Tg2576/CD36^{wt/wt}$	74 ± 6	33.4 ± 2.7	131.1 ± 9.5	7.34 ± 0.02	5
	$Tg2576/CD36^{0/0}$	74 ± 3	30.5 ± 2.1	133.7 ± 9.7	7.36 ± 0.01	5
	$CD36^{0/0}$	81 ± 4	34.2 ± 2.4	134.3 ± 12.1	7.38 ± 0.03	6
22 mo	$CD36^{wt/wt}$	78 ± 3	31.7 ± 1.7	134.7 ± 7.8	7.38 ± 0.01	5
	$Tg2576/CD36^{wt/wt}$	70 ± 7	30.4 ± 2.3	138.4 ± 7.0	7.38 ± 0.04	5
	$Tg2576/CD36^{0/0}$	71 ± 3	34.3 ± 2.8	132.8 ± 8.3	7.37 ± 0.01	5
	$CD36^{0/0}$	81 ± 4	33.9 ± 3.2	130.5 ± 12.2	7.38 ± 0.03	6
A23187, SNAP						
3 mo	$CD36^{wt/wt}$	82 ± 2	32.7 ± 1.5	128.0 ± 4.8	7.37 ± 0.07	5
	$Tg2576/CD36^{wt/wt}$	81 ± 3	34.6 ± 1.4	130.1 ± 6.3	7.35 ± 0.02	5
	$Tg2576/CD36^{0/0}$	81 ± 5	33.8 ± 1.8	134.8 ± 6.4	7.37 ± 0.01	5
	$CD36^{0/0}$	82 ± 4	32.1 ± 4.1	134.5 ± 5.7	7.36 ± 0.02	6
18 mo	$CD36^{wt/wt}$	81 ± 2	35.6 ± 1.5	127.6 ± 4.7	7.38 ± 0.02	5
	$Tg2576/CD36^{wt/wt}$	72 ± 10	33.1 ± 2.9	134.2 ± 8.9	7.35 ± 0.01	5
	$Tg2576/CD36^{0/0}$	73 ± 4	30.8 ± 2.2	137.3 ± 9.8	7.36 ± 0.01	5
	$CD36^{0/0}$	81 ± 4	34.2 ± 2.4	134.3 ± 12.2	7.38 ± 0.02	6
22 mo	$CD36^{wt/wt}$	82 ± 6	31.0 ± 1.3	132.2 ± 4.3	7.38 ± 0.01	5
	$Tg2576/CD36^{wt/wt}$	70 ± 2	32.9 ± 4.7	136.1 ± 9.2	7.38 ± 0.02	5
	$Tg2576/CD36^{0/0}$	70 ± 4	35.6 ± 1.8	132.4 ± 6.6	7.37 ± 0.02	5
	$CD36^{0/0}$	81 ± 2	34.7 ± 2.2	128.2 ± 7.33	7.39 ± 0.03	6
Hypercapnia						
3 mo	$CD36^{wt/wt}$	82 ± 2	54.3 ± 1.5	133.4 ± 4.5	7.23 ± 0.01	5
	$Tg2576/CD36^{wt/wt}$	80 ± 3	56.2 ± 1.1	134.6 ± 6.5	7.18 ± 0.02	5
	$Tg2576/CD36^{0/0}$	80 ± 6	54.3 ± 1.9	134.6 ± 4.5	7.19 ± 0.02	5
	$CD36^{0/0}$	81 ± 3	55.4 ± 2.2	134.9 ± 5.3	7.18 ± 0.01	6
18 mo	$CD36^{wt/wt}$	82 ± 2	56.2 ± 2.1	129.1 ± 6.1	7.22 ± 0.02	5
	$Tg2576/CD36^{wt/wt}$	72 ± 8	54.0 ± 1.3	131.7 ± 7.6	7.17 ± 0.01	5
	$Tg2576/CD36^{0/0}$	73 ± 3	53.9 ± 3.0	137.9 ± 8.8	7.14 ± 0.02	5
	$CD36^{0/0}$	80 ± 4	54.5 ± 4.0	133.2 ± 5.0	7.20 ± 0.01	6
22 mo	$CD36^{wt/wt}$	82 ± 3	53.5 ± 1.8	133.4 ± 7.6	7.20 ± 0.01	5
	$Tg2576/CD36^{wt/wt}$	71 ± 7	52.4 ± 1.7	133.8 ± 7.1	7.19 ± 0.02	5
	$Tg2576/CD36^{0/0}$	73 ± 3	55.5 ± 3.2	129.2 ± 6.0	7.15 ± 0.01	5
	$CD36^{0/0}$	80 ± 4	52.4 ± 4.4	132.4 ± 6.4	7.20 ± 0.01	6

Data are mean ± SEM.